Revision 2

Fluid inclusions examination of the transition from magmatic to hydrothermal conditions in San Diego County, California, pegmatites

Elizabeth M. Gammel and Peter I. Nabelek
Department of Geological Sciences
University of Missouri
Columbia, MO 65211
USA

Correspondence:
Elizabeth Gammel
Department of Geological Sciences
University of Missouri
Columbia, MO 65211

e-mail: egammel@gmail.com
tel: 573-882-8480

ABSTRACT

Thermometric properties and compositions of fluid inclusions in quartz are used to constrain the roles that fluid-soluble elements, principally Li, B, Cl, and F, have in controlling the transition from magmatic to hydrothermal mineral paragenesis in pegmatites and to ultimately understand why some pegmatites in the San Diego County pegmatite district contain abundant, gem-quality, Li-bearing minerals in pockets, whereas others do not. In this district, lithium–cesium–tantalum type pegmatites occur in the Mesozoic Peninsular Ranges Batholith. Emplacement of the dikes occurred at low pressures (200–300 MPa) that resulted in the formation of large miarolitic cavities (pockets), some of which contain gem-quality, Li-bearing minerals. Two pegmatite suites were studied: the gem-bearing Himalaya and the more barren La Posta.

The inclusions measured in this study further underscore highly undercooled crystallization of pegmatites. Pressure-corrected homogenization temperatures (T_h) of c. 400 to 515 °C and c. 270 to 425 °C, were obtained for primary inclusions in the intermediate zone and the core, respectively, of a La Posta dike. Primary inclusions in the intermediate zone and the massive quartz core of the Himalaya pegmatite have T_h ranges of c. 350 to 420 °C and c. 150 to 300 °C, respectively. The high portion of the latter temperature range is interpreted to represent the conditions that existed during the initial crystallization of minerals that line pegmatite pockets.

The most important cations in fluid inclusions in both pegmatites are Na^+, B^{3+}, and Li^+. Lithium concentrations are much higher in inclusions in the Himalaya pegmatite, up to 51 at% of all cations within the massive quartz in the core zone. In the La Posta pegmatite, few primary inclusions contain appreciable Li. The B content of inclusions in

both pegmatites is high, up to 65 at% of cations. The dominant anions in the inclusions are Cl^-, F^- and SO_4^{2-}. The data suggest that hydrothermal fluids that collected in pockets were acidic and promoted the growth of tourmaline and other minerals that are stable in acidic solutions.

In both pegmatites, Na and B dominate secondary inclusions. These inclusions reveal fluids stripped of Li and K by crystallization of lepidolite within fractures of primary minerals throughout the pegmatites, and sometimes as an alteration product in pockets. The lowering of alkali/H^+ ratios in the fluids stabilized clays, including kaolinite, that line the walls of pockets. Coeval crystallization of terminated quartz crystals with clays is consistent with its precipitation from the fluids.

Keywords: pegmatite; Li; B; F; San Diego County, California; pocket minerals

INTRODUCTION

Granitic pegmatites are characterized by large, interlocking crystals up to several meters in length. Pegmatites are generally emplaced as meter to decameter-scale sheets into relatively cold country rocks, therefore, cooling must occur rapidly (Webber et al. 1999; Sirbescu et al. 2008). High water contents and concentrations of fluxing, fluid-soluble elements facilitate both emplacement (due to lowered viscosity) and undercooled crystallization of pegmatite melts (Sirbescu and Nabelek 2003a; Nabelek et al. 2010). In particular, high H_2O contents in silicate melts hinder crystal nucleation and depress the glass transition (T_{gl}) temperature hundreds of degrees (Dingwell et al. 1996; Whittington et al. 2009). Fluxing components that are common in granitic pegmatites, including Li, B, and F, further promote high H_2O solubility and depolymerization of silicate melts (Bailey 1977; London 1984; Dingwell and Webb 1992; Holtz et al. 1993; Veksler and Thomas 2002; Nabelek et al. 2010; Thomas and Davidson 2012; and Bartels et al. 2013). Consequently, very depressed T_{gl} can potentially permit a transition from magmatic to hydrothermal mineral paragenesis at hundreds of degrees below the equilibrium solidus of pegmatite melts. The role of Cl is less known, although it is typically the most abundant anion in exsolved fluids.

The crystallization of minerals that characterize lithium–cesium–tantalum (LCT) type pegmatites is controlled by Li and B (Černý and Ercit 2005). B promotes crystallization of tourmaline, including the schorl and elbaite varieties. Lithium is incompatible with respect to quartz, feldspars, and schorl tourmaline (Brenan et al. 1998; Maloney et al. 2008). Thus, it is concentrated by fractional crystallization in residual liquids. Elevated Li concentrations then promote crystallization of lepidolite, spodumene,

and elbaite tourmaline in cores and along walls of large miarolic cavities or "pockets." The pockets form by accumulation of H_2O. This, combined with relatively low lithostatic pressures, prevents collapse of the pockets. In contrast, high confining lithostatic pressures exerted on deep-seated pegmatites prevent formation of pockets. Pockets of accumulated fluid allow unimpeded growth of crystals. Large crystals in pockets are often wrapped in clays, including kaolinite, cookeite, and montmorillonite (Foord et al. 1986). The clays have previously been attributed to alteration that was unrelated to crystallization of pegmatites (e.g., Foord et al. 1986; Fabre et al. 2002). Foord et al. (1986) suggested a transition from alkaline to acidic conditions as a post-crystallization, supergene process. However, in view of the recognition that pegmatites often crystallize at very low temperatures, we argue in this contribution that clays crystallize at the end of a paragenetic sequence that begins with crystallization of minerals from silicate melts and ends with crystallization of minerals from hydrothermal fluids in pockets.

This study utilizes microthermometric and chemical analysis of fluid inclusions and alteration minerals to understand the role of fluid-soluble elements in the transition from magmatic to hydrothermal crystallization in the Himalaya and La Posta pegmatite suites in San Diego County, California (Figure 1). Both pegmatite suites contain zoned, LCT-type dikes that were emplaced in crystalline rocks of the Peninsular Ranges batholith. However, the two suites are different in that Himalaya pegmatites contain abundant Li-bearing minerals in cores and pockets, whereas in La Posta pegmatites these minerals are uncommon. We compare the microthermometric and compositional properties of primary and secondary fluid inclusions among the pegmatites. Primary inclusions represent trapped fluids that were present during crystallization of minerals

from melts or fluids, whereas secondary inclusions represent fluids that passed through minerals after crystallization and were trapped in healed fractures. Thus, primary and secondary inclusions record fluid evolution through different stages of pegmatite crystallization and alteration.

GEOLOGIC SETTING

San Diego and Riverside Counties of southern California host many pegmatite intrusions that occur within gabbroic and granitic rocks of the Peninsular Ranges batholith (PRB) and included schists. The batholith extends over 1000 km N-S and averages 100 km in width (Figure 1; Walawender and Smith 1980; Smith et al. 1983). The PRB is a Mesozoic continental arc with distinct western and eastern zones. These zones reflect the inferred basements, an oceanic lithosphere in the west and a transitional, continental lithosphere in the east (Wetmore et al. 2002). The western zone of the PRB consists primarily of I-type gabbros, quartz diorites, tonalites, granodiorites, and monzogranites with ages 120 to 105 Ma. Rock types in the eastern zone are I- and S-type tonalites and monzogranites with ages <105 Ma (Walawender et al. 1990). The central zone of the PRB contains a belt of concentrically zoned granitic to tonalitic plutons (90-100 Ma) that are referred to as La Posta-type plutons (Symons et al. 2003). Typically, the plutons grade inward from tonalites to two-mica granites. Pegmatites in San Diego county intruded into these La Posta-type plutons. Paleomagnetic dating of some pegmatites gave ages ca. 94 ± 2 Ma, placing them at the latest stages of magmatism in the PRB (Symons et al. 2009).

STRUCTURE, COMPOSITION, AND CRYSTALLIZATION OF PEGMATITES

Fourteen pegmatite districts occur in San Diego and Riverside Counties (Figure 1). Each of the districts contains hundreds of distinct pegmatite dikes, but only a small fraction of them is considered economically viable, having gem-quality crystals (Fisher 2002). Although the pegmatites are considered to be LCT-type, they contain little Cs and Ta. The pegmatites occur as dikes and dike complexes and show consistent intrusive and morphologic structures. The dips of dikes range from horizontal to ~30°. (We refer to the pegmatites as dikes, because they are typically discordant with respect to the host rocks). By determining the pressure correction necessary to match fluid inclusion homogenization temperatures with oxygen isotope exchange thermometry for pockets, Taylor et al. (1979) estimated the pressure of emplacement of the dikes to have been ~210 MPa.

The typical structure of a San Diego County pegmatite consists of a layered, fine-grained aplite at the lower contact, which is usually absent at the upper contact. Oscillating changes in mineralogy, from quartz and feldspar-rich bands to tourmaline (sometimes garnet)-rich bands, are characteristic of the aplites; hence, the aplites are often referred to as “line rocks”. The crystallization process that resulted in the banding is attributed to the development of boundary layers at propagating crystallization fronts (Rockhold et al. 1987; Webber et al. 1997).

Intermediate zones are present in both the upper and lower halves of dikes and are defined by coarse-grained, inward-pointing, elongated crystals. The crystals, including quartz, microcline, plagioclase, and schorl tourmaline, typically range in size from centimeters to decimeters. Graphic intergrowths of microcline and quartz are common.

The morphologies of crystals in intermediate zones point to in-situ, inward crystallization and rapid cooling of dikes (London 2009).

Centers of dikes may or may not contain core zones. Core zones consist of massive crystals and may contain small, usually barren pockets. Core zones themselves may be mostly "barren", consisting mostly of quartz and interstitial feldspar, or may be "fertile", containing also Li-bearing and other minerals. However, most gem-quality, terminated crystals are found in pockets that occur directly between lower and upper intermediate zones. Zeolites, clays, and other low-temperature, hydroxyl-bearing minerals are abundant in these pockets as alteration products of Li-bearing minerals or as minerals grown on pocket walls (Foord et al. 1986). Spodumene, in particular, is commonly altered to cookeite. Clays also occur as inclusions within euheral quartz crystals. In the paragenetic sequence of clays proposed by Foord et al. (1986), cookeite is the earliest and kaolinite is the latest.

From oxygen isotope exchange thermometry among coexisting minerals, Taylor et al. (1979) estimated that crystallization temperatures ranged from 700-730 °C at pegmatite margins to 525-565 °C in the pockets. The estimates require, however, the assumption that oxygen isotope exchange achieved equilibrium at the temperatures of crystallization, which may not necessarily be the case for crystallization in undercooled dikes. Taylor et al. (1979) obtained uncorrected homogenization temperatures of fluid inclusions in pocket minerals ranging from 255 to 340 ºC.

La Posta pegmatites

La Posta pegmatites of the Jacumba district intruded the tonalitic to granodioritic La Posta pluton. The district consists of many, several-meters thick dikes and thinner veins that run parallel to one another and dip slightly to the south-southwest. Samples described here are from a dike closest to the eastern edge of the La Posta pluton, which is tonalitic at this location.

La Posta pegmatites display the characteristic morphology of pegmatite dikes, having line rocks, intermediate zones, and quartz cores. They are not actively mined at present, but gem-quality spessartine garnet and smoky quartz were found in the past (Fisher 2002). Secondary micas occur along fractures throughout the dikes. Quartz cores in La Posta pegmatites are largely barren. Large pockets are common, but they generally lack Li minerals. Clays and other low-temperature minerals are rare in La Posta pegmatites.

Himalaya pegmatite

The Himalaya pegmatite dikes in the Mesa Grande district intruded into a gabbronorite host rock (Fisher 2002). Two pegmatite dikes converge at the San Diego mine where samples were collected. Here the dikes are up to 2 m thick (Webber et al. 1999). The dikes are tabular and dip slightly to the west and southwest and can be traced for a distance of ~900 m (Fisher et al. 1998).

Himalaya dikes are mineralogically more complex than La Posta dikes, particularly with respect to cores and pockets. Portions of Himalaya dikes include core zones, some of them barren and some fertile with elbaite tourmaline, spodumene and lepidolite. However, most gem-quality minerals occur in pockets within intermediate

zones. Zeolites, clays, and other low-temperature minerals are common in these pockets. Thus, Himalaya dikes contain high abundances of both Li-bearing primary minerals and clays, whereas La Posta dikes are poor in both. Mica fracture fillings also appear to be more extensive in Himalaya dikes than in La Posta dikes.

METHODS AND SAMPLE COLLECTION

Samples

Fluid inclusion data reported here come from quartz that was collected in intermediate zones and cores of one La Posta dike and one Himalaya dike. The La Posta samples come from the upper intermediate zone of an approximately 5 m thick dike and its barren core. The Himalaya samples come from the intermediate zone in the center of a dike next to a pocket and from a barren core that occurs some distance from the pocket along strike. The core contains small barren pockets. Of twenty-three doubly-polished thick-sections, ten from the La Posta pegmatite and seven from the Himalaya pegmatite were chosen for analysis of fluid inclusions.

Cathodoluminescence (CL) microscopy and SEM analysis

All thick-sections were analyzed using a cold cathode, CITL Mk5 cathodoluminescence system mounted on an Olympus BX51 petrographic microscope. Samples were exposed to the electron beam for durations ranging between seconds and minutes in order to observe possible trace element zoning in minerals, secondary minerals filling microfractures in primary minerals, and alteration of minerals hosting the microfractures. All samples were analyzed using 15 keV accelerating voltage. Mineral

identification was aided by back-scatter electron (BSE) and energy-dispersive X-ray analyses (EDS) using a FEI Quanta 600 scanning electron microscope (SEM).

Microthermometry

After petrographic and CL analyses, thick-sections were removed from the glass slides and broken into chips <6 mm in diameter. Heating and freezing of fluid inclusions was conducted on a Linkham THMSG 600 computer-controlled, heating-freezing stage with a range of –198 to 600 ºC. It was calibrated using phase transitions of natural and synthetic pure CO_2 and H_2O inclusions. Individual inclusion assemblages in quartz were first heated to homogenization, subsequently cooled to –150 ºC, and then slowly reheated to record phase transition temperatures. Temperatures were collected for homogenization (T_h), eutectic melting (T_e) and last ice melting (T_m). The data are reported in Supplementary Materials.

Laser-ablation ICP-MS

Laser-ablation inductively coupled plasma mass spectrometry (LA-ICP-MS) was used to obtain elemental compositions of fluid inclusion assemblages that were previously analyzed by microthermometry. Additionally, host quartz was qualitatively analyzed for trace element abundances. Fluid inclusion data were collected at the Fluid Research laboratory of the Virginia Polytechnic Institute and State University using an Agilent 7500ce ICP-MS coupled with a Geolas laser ablation system. Analysis of a set of three to four chips was bracketed by analysis of the NIST-610 glass standard. Standard

246 deviations on repeated analysis of the standard are: Li – 2.4 %, B – 1.2 %, Na – 1.5 %, K
247 – 1.0 %, Ca – 3.6 %, Sr – 0.8 %.

248 After 60 seconds of collecting background data, the laser beam was unblocked
249 and ablation began until inclusions were encountered. Attempts were made to detect Li,
250 Be, B, Na, Mg, Al, K, Ca, Mn, Fe, Rb, Sr, Sn, Cs, Ba, and W in each inclusion, but only
251 Li, B, Na, K, Ca and trace Cs, Be, Fe, Rb, Sr, Ba, and W were above the detection limits.
252 Raw time-series data were reduced using the AMS software that couples LA-ICP-MS
253 data with microthermometric measurements (Mutchler et al. 2008). The software
254 incorporates the data reduction procedure of Longerich et al. (1996). It takes into account
255 the background information collected on each sample as well as data for standards. Peak
256 positions from fluid inclusion extractions were manually picked. Solute concentrations
257 equivalent to wt% of NaCl ($NaCl_{eq}$) were calculated within the software based on
258 calibrations of Heinrich et al. (2003). Mineral analyses were conducted at the University
259 of Missouri Research Reactor with a NexION 300X ICP-MS coupled to an Analyte 193
260 nm ultra-short pulse excimer laser.
261

262 **Ion chromatography**

263 Fluid inclusions extracted using the crush-leach technique (Banks and Yardley
264 1992) were analyzed for anions using the Dionex ICS-3000 Ion Chromatography System.
265 Limits of detection (LOD) and standard deviation of peak area for fluoride, chloride, and
266 sulfate were calculated from 12 analyses of standards with concentrations ranging from
267 0.042 to 2.63 mM fluoride, chloride, and sulfate concentrations. Fluoride LOD was
268 calculated at 0.089 mM and the standard deviation in peak area was 0.077. For chloride,

LOD was 0.093 mM with a peak area standard deviation of 0.082, and sulfate LOD was 0.031 mM with 0.018 standard deviation in peak area.

Ten La Posta and six Himalaya samples were analyzed. Other minerals that were attached to quartz were physically separated and discarded so that only quartz remained. The samples were cleaned before leaching using repeated nitric acid washing and extraction in an ultrasonic bath using a technique similar to that of Channer et al. (1999). Sequential nitric acid washes were also analyzed to determine the effectiveness of sample cleaning prior to crushing of each sample.

A standard with 0.1 mM concentration of each of F, Cl, N, Br, N, P, S was used to bracket sample analyses. Each sample leachate was run twice. Analyzed volumes of samples, standard, and blanks were all 0.5 mL. Data were reduced by the Dionex Chromeleon chromatography management system. Standard deviations of unknowns were calculated from multiple runs of the same fluid extract.

RESULTS

Cathodoluminescence

Cathodoluminescence petrography reveals similar features in both pegmatites. Microcline exhibits blue and plagioclase exhibits green luminescence. Micas vary from non-luminescing biotite to deep-red luminescing lepidolite (Figure 2a). Gorobets and Rogojine (2002) cited Fe^{3+} as a possible emitter for the pink 700-725 nm CL wavelength from lepidolite. Edgington (1970) noted that muscovite emits an inherent wavelength of 680 nm. Quartz shows little to no luminescence except in >1 minute exposures. When

quartz does luminesce, it is pale blue (Figure 2b), which is typical for quartz of igneous origin (Marshall 1988).

Minerals filling fractures throughout the samples display the pink luminescence that is characteristic of lepidolite (Figure 2b, c, d). The identity of pink-luminescing lepidolite as a mica was confirmed by SEM images that clearly show the {001} cleavage. In tourmaline, fractures and fracture fillings are larger and more intense under CL than the same fractures in neighboring minerals. Figure 2d shows how CL of fracture-fillings emanating from quartz intensify in tourmaline. Lepidolite in tourmaline also contains measurable amounts of Mn.

Quartz adjacent to fractures displays a more pronounced blue color. LA-ICP-MS analysis shows elevated Li and Al in the blue regions. The blue color is not symmetric about the fractures, which is attributed to oblique orientations of the fractures relative to surfaces of thick sections. Bright blue luminescence in quartz (460-490 nm light; Figure 2b) is attributed to crystal defects resulting from $Si^{4+} \rightarrow Al^{3+} + Li^{+}$ substitution (Marshall 1988; Luff and Townsend 1990; Xu et al. 2001; Botis and Pan 2011). This substitution has been documented in several LCT pegmatites in northeastern Brazil (Beurlen et al. 2011).

Feldspars near fractures show a dull brown luminescence that is indicative of secondary alteration. The alteration is more extensive around fracture networks within grains (Figure 2c). The luminescence (610-625 nm) is attributed to Eu^{3+} (Gaft et al. 1998).

Microthermometry

Fluid inclusions in the pegmatites usually occur in assemblages that are defined by similar petrographic and microthermometric properties of inclusions. Primary inclusions were identified as those occurring in small clusters and not along healed fractures (Figure 3a). Primary inclusions typically range in size from 20 to 50 μm. Secondary inclusions are generally smaller, 10 to 25 μm, and occur along healed fractures that often cross crystal boundaries (Figure 3b). Secondary inclusions represent the majority of inclusions in most samples, except in the core of the Himalaya pegmatite, in which primary inclusions dominate. Measurements on over 100 primary and secondary inclusions were made. All inclusions contain an aqueous liquid + vapor assemblage and all, except two, homogenized to liquid upon heating. No CO_2 was observed optically in the inclusions, although Taylor et al. (1979) were able to extract minor amounts of CO_2 from crushed inclusions in a vacuum line during preparation for stable isotope measurements.

Himalaya Pegmatite. Figure 4a shows homogenization and eutectic melting temperatures of all measured inclusions in the intermediate zone and the core. Primary inclusions in the intermediate zone homogenized between 202.1 and 270.7 ºC, and have T_e's from –63.1 to –21.8 ºC. Primary inclusions in the core have lower homogenization temperatures, 101.8 to 151.9 ºC. Eutectic temperatures range from –45.4 to –24.7 ºC. Eutectic temperatures below that of the NaCl-H_2O system show the presence of solutes in addition to NaCl. Secondary inclusions in the intermediate zone homogenized between 124.7 and 292.7 ºC and T_e's are from –28.3 to –12.1 °C. The T_h's of secondary inclusions in the intermediate zone span the whole range of primary inclusions, suggesting that they

were trapped throughout crystallization of the pegmatite. However, the narrower range of eutectic temperatures indicates less complex combinations of solutes that in the primary inclusions.

Last ice melting temperatures give an accurate indication of the salinity of aqueous inclusions when the solute is only NaCl. For inclusions with complex combinations of solutes, derived salinities (wt%) are only approximate, here reported as $NaCl_{eq}$. In most inclusions in the pegmatite, T_m ranges from –13.1 to –0.9 ºC, corresponding to solute concentrations of 17.0 to 1.6 $NaCl_{eq}$. This range is similar for primary and secondary inclusions. Two secondary inclusions had markedly lower T_m's of –24.6 and –20.5 ºC, corresponding to 25.3 and 22.7 $NaCl_{eq}$, respectively.

La Posta pegmatite. Ten samples from the La Posta pegmatite were analyzed for fluid inclusions. Primary inclusions in the intermediate zone display the highest T_h's, 254.8 to 367.6 ºC, and the lowest T_e's, –67.4 to –21.9 ºC , but the majority is between –50 and –40 °C (Figure 4b). The low T_e's indicate the presence of other solutes besides NaCl. In the core, T_h of primary inclusions ranges from 123.2 to 275.8 ºC. Eutectic temperatures in these inclusions range from –44.8 to –14.1 ºC. On average, T_e's of primary inclusions indicate a different combination of solutes in the intermediate zone than in the core, most likely a significant concentration Ca in the intermediate zone.

Secondary inclusions in the intermediate zone have T_h's from 193.8 to 286.5 ºC and T_e's from –30.2 to –12.4 ºC. Homogenization temperatures of secondary inclusions in the core range from 119.8 to 280.1 °C, and T_e's range from –46.4 to –12.3 ºC. These ranges for the core effectively correspond to those of primary inclusions.

Cations in fluid inclusions

Concentrations of cations in fluid inclusions obtained by LA-ICP-MS are given in Supplementary Materials and are presented in atomic proportions relative to all detected cations in Figure 5. The most abundant cations in the inclusions are Na, B, Li and Ca. Small amounts of Cs occur in nearly all inclusions, and some additional cations were detected sporadically.

Himalaya pegmatite. In the Himalaya pegmatite, the three analyzed primary inclusions in the intermediate zone are dominated by Na and contain only small proportions of B and Li (Figure 5a). These inclusions also contain 2–6 at% Ca and 1–2 at% Cs. Inclusions in the barren core contain the highest proportions of Li of all measured inclusions. These inclusions have no measurable Ca, except for one inclusion, but contain trace Cs (0.04–0.2 at%).

Secondary inclusions in the intermediate zone contain no measurable Li and have large variations in the B/Na ratio. The range in the B/Na ratios is reflected in the range of T_e's, many of which are above the T_e of the NaCl-H_2O system. These inclusions also contain 1–5 at% Ca and up to 1 at% of Cs.

La Posta pegmatite. Most La Posta inclusions contain very little or no measurable Li but contain higher concentrations of Ca than Himalaya inclusions (Figure 5c-d). Only two primary inclusions contained measurable Li. Primary inclusions in the intermediate zone also contain K (3-6 at%) and Cs (~0.1 at%). Primary inclusions in the

core contain equivalent atomic proportions of Na and B. Traces of Cs (0.05 at%) occur in these inclusions as well. W (0.02 at%) was detected in one inclusion.

Secondary inclusions in the intermediate zone contain up to 10 at% Ca, up to 13 at% K, but most have no measurable Li. These inclusions also contain <1 at% Cs. Secondary inclusions in the core contain some of the highest relative concentrations of Ca. These inclusions also contain 6–7 at% K, trace Cs (0.04 at%), and Sr (0.13 at%).

Ion chromatography

Analysis of crush-leached inclusions permits obtaining only relative proportions of anions. They are reported here as ratios. Crush-leaching extracts primary and secondary inclusions together, thus the technique cannot distinguish anions in the two types of inclusions. Because secondary inclusions are more prevalent in the pegmatites, the measured anion concentrations are more representative of secondary fluids.

In the Himalaya pegmatite, F^-/Cl^- and SO_4^{2-}/Cl^- ratios do not show a distinct difference between inclusions in the intermediate zone and the core zone (Figure 6). However, the ratios show 8% F^- and 4.5% SO_4^{2-} in the fluids. Similar F^-/Cl^- and SO_4^{2-}/Cl^- ratios occur in inclusions within the core of the La Posta pegmatite. However, inclusions in the intermediate zone have up to 18% F^- and 9% SO_4^{2-}. Both of these anions occur in acids, and thus indicate that the trapped fluids (mostly secondary) were acidic.

Trapping temperatures

406 Measured T_h's of primary inclusions in the two pegmatites (Figure 4a, b) would
407 suggest crystallization not only below the equilibrium solidus temperature of a H_2O-
408 saturated granite melt, but also below its glass transition temperature (Nabelek et al.
409 2010). Measured T_h's of fluids represent the minimum trapping temperatures because
410 they do not include isochoric corrections for pressure. Because all analyzed inclusions
411 homogenized to liquid, their isochores are most likely steep in *P*-*T* space. However,
412 isochores for complex inclusions that include B cannot be accurately calculated due to
413 the lack of equations of state for B-bearing fluids; therefore, pressure corrections for
414 individual inclusions were not made. The pressure correction was roughly estimated from
415 inclusions containing >70 atomic % Na relative to all other cations present by using an
416 equation of state of Bodnar and Vityk (1994). Only secondary inclusions in the
417 pegmatites contain such high proportions of Na. Based on five inclusions and assuming
418 the 200–300 MPa pressure range for emplacement of the pegmatites, the pressure
419 correction results in 110 to 180 ºC higher trapping temperatures than the observed
420 homogenization temperatures. The correction brings T_h's of all primary inclusions in
421 intermediate zones above T_{gl} of H_2O-saturated melts (Nabelek et al. 2010).
422 Most primary inclusions in massive quartz cores have T_h's that even with the
423 pressure correction are below T_{gl} (Figure 4a). In the core of the Himalaya pegmatite,
424 inclusions also have very low T_e's (approximately –40°C), which is predicted for fluid
425 containing ≥20 wt% LiCl (Dubois et al. 2010). LA-ICP-MS data show that these
426 inclusions contain up to 50 at% Li. A study by Mao and Duan (2008) shows that
427 isochores of LiCl-bearing fluids have similar *P*-*T* slopes as NaCl-bearing fluids, thus the
428 pressure correction for trapping temperatures is similar to NaCl-rich inclusions. Because

the corrected temperatures remain below T_{gl}, they indicate that quartz cores crystallized from hydrothermal fluids. However, high B concentrations in inclusions trapped in quartz cores bring an additional uncertainty to the pressure correction.

DISCUSSION

The paragenesis of minerals in the Himalaya and La Posta pegmatites is reflected in the evolution of trapped fluids. Microthermometric and LA-ICP-MS data distinguish primary and secondary fluid inclusions and are used to interpret stages in crystallization of the pegmatites.

Implications for crystallization of pegmatite melts

Pressure corrected homogenization temperatures (ca. 380–580 ºC) suggest both the La Posta and Himalaya pegmatites crystallized at temperatures below the typical granite solidus (Figure 4). Previous research shows undercooled crystallization is typical of granitic pegmatites (London 1986; Webber et al. 1999; Sirbescu and Nabelek 2003a; Sirbescu et al. 2008; Nabelek et al. 2010). Large amounts of water that were dissolved in the pegmatite melts probably played the major role in the undercooled crystallization of the La Posta and Himalaya pegmatites; however, the considerable amounts of B, Li, and F that the pegmatite melts contained probably increased the solubility of water in the melts further and aided in their depolymerization (London 1984; Holtz et al. 1993; Veksler and Thomas 2002; Nabelek et al. 2010; Thomas and Davidson 2012; and Bartels et al. 2013). The pressure-corrected trapping temperatures of primary inclusions in intermediate zones of the pegmatites give an indication of the lower end of the

452 temperature range in which crystallization from the pegmatite melts has occurred.
453 Oxygen isotope exchange thermometry in aplites (Taylor et al., 1979) gives the best
454 indication of the upper end of the crystallization temperature range. Despite the fact that
455 large crystals occur in pegmatite cores, pressure-corrected homogenization temperatures
456 (ca. 200–330 ºC) remain below the glass transition temperature, which is strong evidence
457 of a transition to mineral crystallization from a hydrothermal fluid rather than a melt (c.f.,
458 Thomas and Davidson, 2012).
459
460 **Controls of Li and B on mineralogy**
461 The presence of Li and B in pegmatite melts causes crystallization of minerals
462 that characterize LCT pegmatites. In accord with published experimental data (e.g.,
463 Dubois et al. 2013), the measured fluid inclusions show that both elements are soluble in
464 H_2O. Lithium is typically complexed with Cl and B probably occurs as boric acid
465 (Williams and Taylor 1996). However, B and Li are used differently during
466 crystallization of pegmatites. Boron is used by tourmaline throughout crystallization, in
467 line rocks, in intermediate zones, in cores, and in pockets. On the other hand, even when
468 occurring in relatively high concentrations as in the Himalaya pegmatite, minerals in
469 which Li is an essential structural constituent, such as lepidolite, spodumene, and elbaite
470 tourmaline, occur only in cores and pockets. In accord with observations from other
471 pegmatite dikes in San Diego County (Maloney et al. 2008), Li becomes concentrated by
472 fractional crystallization and fluid accumulation in centers of dikes where Li-bearing
473 minerals then crystallize. Accumulation of Li in centers of dikes and along secondary
474 fractures in the form of lepidolite (Figures 2b, c, and d) is demonstrated by primary

475 inclusions in the core of the Himalaya pegmatite. Contrastingly, the smaller abundance of
476 Li in La Posta fluid inclusions, including in its core zone, suggests why Li minerals are
477 uncommon in La Posta dikes (Figure 5a and c).
478
479 **Origin of Ca in La Posta pegmatites**
480 Proportionally higher Ca concentrations and smaller Li concentrations in
481 inclusions of the La Posta pegmatite are the major chemical differences that distinguish
482 its inclusions from those in the Himalaya pegmatite. Elevated Ca was measured (Figure
483 5) and is indicated by very low T_e's (Figure 6) of primary inclusions in the intermediate
484 zone of the La Posta pegmatite, which suggests that Ca was a component in the pegmatite
485 melt, rather than a product of post-crystallization alteration as proposed by Foord et al.
486 (1986) for the occurrence of Ca minerals, such as laumontite and zeolites, in pockets of
487 some pegmatites. Symons et al. (2009) showed that emplacement of the La Posta dikes
488 occurred during the latest stages of growth of the La Posta pluton. The still hot La Posta
489 pluton may have promoted diffusion of Ca into the pegmatite melt as it passed through
490 the pluton. This is supported by Sr in Ca-bearing fluid inclusions (supplementary
491 materials), and lack of Sr in non-Ca-bearing inclusions.
492
493 **Alteration mineralogy and ion-exchange reactions**
494 Similar ranges in Na/B ratios in primary and secondary inclusions in both
495 pegmatites suggest that secondary fluids originated from pegmatite melts and reflect
496 evolution of fluid compositions during cooling. However, the lack of detectable Li in
497 most secondary inclusions suggests that Li was scavenged by lepidolite and other Li-

bearing minerals that crystallized in fracture fillings, fertile cores, and along pocket walls (Figures 2b, c, and d). Tourmaline, being an aluminous mineral, likely undergoes a reaction with the secondary fluid and produces additional lepidolite, as seen in the intensity increase and width of fractures in tourmaline (Figure 2d). The occurrence of lepidolite within fractures and on walls of pockets and the alteration of spodumene to cookeite (Foord et al. 1986) demonstrates that late-stage, Li-enriched fluids were reactive and generated the secondary minerals during subsolidus conditions.

Foord et al. (1986) and Stern et al. (1986) attribute late-stage clays to direct crystallization from late hydrothermal fluids, with kaolinite crystallizing last in the presence of moderately acidic, supergene solutions. We agree that late-stage clays could have precipitated directly from acidic fluids. However, we suggest that the fluids originated from the pegmatites and evolved to more acidic conditions during crystallization of Li minerals, instead of being supergene fluids, unrelated to crystallization of pegmatites.

As shown by Stern et al (1986) and Figure 7, kaolinite is stable relative to alkali feldspars, muscovite and paragonite at the low temperatures that existed in the pockets and with acidic hydrothermal fluids present. For example, the equilibrium relationships between muscovite and kaolinite can be described by the following reaction:

$$2\ KAl_3Si_3O_{10}(OH)_2\ (s) + 3\ H_2O + 2\ H^+\ (aq) = 3\ Al_2Si_2O_5(OH)_4\ (s) + 2\ K^+\ (aq), \quad (1)$$

where the anions are F^-, Cl^-, or SO_4^{2-}, all of which occur in secondary inclusions in the pegmatites (Figure 6). Diagrams of $a_{(Na^+/H^+)}$ *vs. T* and $a_{(K^+/H^+)}$ *vs. T* shown in Figure 7,

were calculated using the computer program SUPCRT (Johnson et al. 1991). We attribute the increase in acidity that was necessary to stabilize kaolinite to scavenging of Li (and K) from the hydrothermal fluid during crystallization of lepidolite and other Li-bearing minerals in pockets. Williams and Taylor (1996) used ionization potentials to identify H_3BO_3 by mass spectrometry in fluid inclusions in Belo Horizonte mine in San Diego County. However, they did not detect H_3BO_3 in the Himalaya pegmatite, though they did not exclude other possible B species. Our analysis shows high proportions of B in all inclusions in the Himalaya pegmatite, thus a B species, possibly H_3BO_3, must have existed in the fluids during crystallization.

The occurrence of clays in pockets of pegmatites requires them to be either alteration products of primary minerals or products of primary crystallization from acidic fluids. Of all elements required to precipitate clays, Al is thought to be the least soluble element in fluids. Recent studies of Al solubilities in hydrothermal solutions suggest that enough Al could be contained in collected pegmatite fluids for direct precipitation of clays to occur (Manning et al. 2010; Wohlers et al. 2011; Galvez et al. 2015). A fluid in equilibrium with albite + paragonite + quartz at 500 °C and 1000 MPa contains ~0.03 mol of Al/kg H_2O and has molar Si/Al ratio of ~8. Assuming that this solubility is applicable to fluids at <300 °C and 200 MPa, a 2×1×1 m column of pegmatite melt with 8 wt% H_2O (Johannes and Holtz 1996) could potentially result in precipitation of 1.5 kg of kaolinite from exsolved fluid. This amount of clay is typical of the amounts in pegmatite pockets. In addition, Newton and Manning (2006) showed that Al solubility in fluid is further enhanced by the presence of Cl. In pockets, euhedral, terminated quartz crystals are commonly surrounded by and contain inclusions of clay. Given the predicted

high Si/Al ratio in hydrothermal fluids, it is unsurprising that quartz and clays would crystallize together during the terminal stages of a mineral paragenetic sequence in a pegmatite dike.

Primary inclusions in core zones containing massive quartz in the Himalaya pegmatite are distinct from others in microthermometry (Figure 4) and chemistry (Figures 5). There exists a sharp boundary between this massive quartz and the overlying intermediate zone. In particular, these inclusions have equivalent concentrations of Li, B, and Na, and fairly high proportions of F^-. We attribute massive quartz core zones not only to inherent high solubility of Si in saline aqueous solutions (e.g. Fournier 1983), but also to complexing with F^-, which may have aided in Si transport and ultimate crystallization of quartz in centers of dikes. Fluid trapped in inclusions in the Himalaya pegmatite core may be representative of fluids that exsolve and collect in pockets of gem-bearing pegmatites The chemical and transport characteristics of such fluids cause crystallization of quartz (± spodumene) cores in pegmatites that intrude at higher pressures wherein pockets cannot develop (e.g., Black Hills, South Dakota; Sirbescu et al. 2003b).

IMPLICATIONS

Fluid inclusion microthermometry and compositions in the Himalaya and La Posta pegmatites support low-temperature crystallization of intermediate zones in the dikes and a continuous mineral paragenesis from magmatic to hydrothermal stages (c.f., London, 1986; Thomas and Davidson 2012). The continuous transition is facilitated by undercooled crystallization of H_2O-enriched intermediate zones. Particularly low

567 homogenization temperatures and high Li and B concentrations in inclusions within the
568 quartz core of the Himalaya pegmatite demonstrate the importance of Li-bearing fluids to
569 crystallization of Li minerals in pockets of many pegmatites in San Diego County.
570 During the hydrothermal stage of pegmatite crystallization, fluids evolve toward acidic
571 conditions by crystallization of alkali-bearing phases, including lepidolite, on walls of
572 pockets. Ultimately, the acidic fluids stabilize clays that characterize the end-stages of
573 mineral paragenesis in pocket-containing pegmatites.
574

575 **ACKNOWLEDGMENTS**

576 We would like to thank Robert Bodnar and Luca Fedele at Virgina Tech and
577 Barry Higgins at the University of Missouri Research Reactor for their help in use of LA-
578 ICP-MS systems. We would also like to thank Mona Sirbescu for her help in the field and
579 organizing the trip to the San Diego County pegmatites. Jim Means and Bill Calhoun
580 kindly allowed us to collect samples in the La Posta and Himalaya pegmatite mines,
581 respectively. Ilia Veksler and an anonymous reviewer provided constructive reviews of
582 the manuscript. Editorial comments by Paul Tomascak improved the contribution. The
583 work was partially funded by NSF grant EAR-1321519.
584

REFERENCES CITED

Bailey, J.C. (1977) Fluorine in granitic rocks and melts: a review. Chemical Geology, 19, 1–42.

Banks, D.A., and Yardley, B.W.D. (1992) Crush-leached analysis of fluid inclusions in small natural and synthetic samples. Geochimica et Cosmochimica Acta, 56, 245–248.

Bartels, A., Behrens, H., Holtz, F., Schmidt, B.C., Fechtelkord, M., Knipping, J., Crede, L., Baasner, A., and Pukallus, N. (2013) The effect of fluorine, boron and phosphorus on the viscosity of pegmatite forming melts. Chemical Geology, 346, 184–198.

Beurlen, H., Muller, A., Silva, D., and Da Dilva, M.R.R. (2011) Petrogenetic significance of LA-ICP-MS trace-element data on quartz from the Borborema Pegmatite Province, northeast Brazil. Mineralogical Magazine, 75, 2703–2719.

Bodnar, R.J. and Vityk, M.O. (1994) Interpretation of microthermometric data for H_2O–NaCl fluid inclusions. De Vivo B. and Frezzotti M.L. (eds) Fluid Inclusions in Minerals: Methods and Applications, 117–130.

Botis, S.M., and Pan, Y. (2011) Modeling of $[AlO_4/Li^+]^+$ paramagnetic defects in α-quartz. Canadian Journal of Physics, 89, 809–816.

Brenan, J.M., Neroda, E., Lundstrom, C.C., Shaw, H.F., Ryerson, F.J., Phinney, D.L. (1998) Behaviour of boron, beryllium, and lithium during melting and crystallization: constraints from mineral-melt partitioning experiments. Geochimica et Cosmochimica Acta, 62, 2129–2141.

607 Černý, P., and Ercit, T.S. (2005) The classification of granitic pegmatites revisited. The
608 Canadian Mineralogist, 43, 2005–2026.
609 Channer, D.M.DeR., Bray, C.J., and Spooner, E.T.C. (1999) Integrated cation-
610 anion/volatile fluid inclusion analysis by gas and ion chromatography:
611 methodology and examples. Chemical Geology, 154, 59–82.
612 Dingwell, D.B., and Webb, S.L. (1992) The fluxing effect of fluorine at magmatic
613 temperatures (600–800 ºC): A scanning calorimetric study. American
614 Mineralogist, 77, 30–33.
615 Dingwell D.B., Hess, K. U., and Knoche, R. (1996) Granite and granitic pegmatite melts:
616 volumes and viscosities. Transactions of the Royal Society of Edinburgh: Earth
617 Sciences, 87, 65–72.
618 Dubois, M., Monnin, C., Castelain, T., Coquinot, Y., Guoy, S., Gauthier, A., and Goffe,
619 B. (2013) Investigation of the H_2O–NaCl–LiCl system: a synthetic fluid inclusion
620 study and thermodynamic modeling from –50º to +100 ºC and up to 12 mol/kg.
621 Economic Geology, 105, 329–338.
622 Edgington, J.A., and Blair, I.M. (1970) Luminescence and thermoluminescence induced
623 by bombardment with protons of 159 million electron volts. Science, 167, 715–
624 717.
625 Fabre, C., Boiron, M.C., Dubessy, J., Chabiron, A., Charoy, B., and Crespo, T. (2002)
626 Advances in lithium analysis in solids by means of laser-induced breakdown
627 spectroscopy: An experimental study. Geochimica et Cosmochimica Acta, 66,
628 1401–1407.

629 Fisher, J., Foord, E.E., and Bricker, G.A. (1998) The geology, mineralogy, and history of
630 the Himalaya Mine, Mesa Grande, San Diego County, California. Rocks and
631 Minerals, 156–180.
632 Fisher, J. (2002) Gem and rare-element pegmatites of southern California. Mineralogical
633 Record, 33, 363–407.
634 Foord, E.E., Starkey, H.C., and Taggart, J.E. (1986) Mineralogy and paragenesis of
635 "pocket clays" and associate minerals in complex granitic pegmatites, San Diego
636 County, California. American Mineralogist, 71, 428–439.
637 Fournier, R.O. (1983) A method for calculating quartz solubilities in aqueous sodium
638 chloride solutions. Geochimica et Cosmochimica Acta, 47, 579-586.
639 Gaft, M., Reisfeld, R., Panczer, G., Blank, P., and Boulon, G. (1998) Laser-induced time-
640 resolved luminescence of minerals. Spectrochimica Acta-Part A: Molecular and
641 Biomolecular Spectroscopy, 54, 2163–2175.
642 Galvez, M.E., Manning, C.E., Connolly, J.A.D. & Rumble, D. (2015) The solubility of
643 rocks in metamorphic fluids: A model for rock-dominated conditions to upper
644 mantle pressure and temperature. Earth and Planetary Science Letters, 430, 486–
645 498.
646 Gorobets, B.S., and Rogojine, A.A. (2002) Luminescent Spectra of Minerals, Coronet
647 Books Inc., Philadelphia, 300 p.
648 Heinrich, C.S., Pettke, T., Halter, W.E., Aigner-Torres, M., Audetat, A., Gunther, D.,
649 Hattendorf, B., Bleiner, D., Guillong, M., and Horn, I. (2003) Quantitative multi-
650 element analysis of minerals, fluid and melt inclusions by laser-ablation

651 inductively-coupled-plasma mass-spectrometry. Geochimica et Cosmochimica
652 Acta., 67, 3473–3496.
653 Holtz, F., Dingwell, D.B., and Behrens, H. (1993) Effects of F, B_2O_3 and P_2O_5 on the
654 solubility of water in haplogranite melts compared to natural silicate melts.
655 Contributions to Mineralogy and Petrology, 113, 493–501.
656 Johannes, W., and Holtz, F. (1996) Petrogenesis and experimental petrology of granitic
657 rocks. Springer, Berlin, p. 335
658 Johnson, J.W., Oekers, E.H., and Helgeson, H.C. (1991) SUPCRT92, a software package
659 for calculating the standard molar thermodynamic properties of minerals, gases,
660 aqueous species, and reactions from 1 to 5000 bars and 0^o to 1000^o C. Livermore.
661 California, Lawrence Livermore Laboratory.
662 London, D. (1984) Experimental phase equilibria in the system $LiAlSiO_4$–Si_2O–H_2O: a
663 petrogenetic grid for lithium-rich pegmatites. American Mineralogist, 69, 995–
664 1004.
665 London, D. (1986) Magmatic-hydrothermal transition in the Tanco rare-element
666 pegmatites: Evidence from fluid inclusions and phase-equilibrium experiments.
667 American Mineralogist, 70, 376–395.
668 London, D. (2009) The origin of primary textures in granitic pegmatites. The Canadian
669 Mineralogist, 47, 697–724.
670 Longerich, H.P., Jackson, S.E., and Cunther, D. (1996) Laser ablation inductively
671 coupled plasma mass spectrometric transient signal data acquisition and analyte
672 concentration calculation. Journal of Analytical Atomic Spectrometry, 11, 899–
673 904.

Luff, B.J., and Townsend, P.D. (1990) Cathodoluminescence of synthetic quartz. Journal of Physics: Condensed Matter, 40, 8089–8097.

Maloney, J.S., Nabelek, P.I., Sirbescu, M.C., and Halama, R. (2008) Lithium and its isotopes in tourmaline as indicators of the crystallization process in the San Diego County pegmatites, California, USA. European Journal of Petrology, 20, 905–916.

Manning, C.E., Antignano, A., and Lin, H.A. (2010) Premelting polymerization of crustal and mantle fluids, as indicated by the solubility of albite+paragonite+quartz in H_2O at 1 GPa and 350–620°C. Earth and Planetary Science Letters, 292, 325–336.

Mao, S., and Duan, Z. (2008) The P, V, T, x properties of binary aqueous chloride solutions up to T = 573 K and 100 MPa. Journal of Chemical Thermodynamics, 40, 1046–1063.

Marshall, D.J. (1988) Cathodoluminescence of Geological Materials. Unwin Hyman Ltd. London, UK, 146 p.

Mutchler, S.R., Fedele, L., and Bodnar, R.J. (2008) Appendix A5: Analysis management system (AMS) for reduction of laser ablation ICP-MS data. Mineralogical Association of Canada: Short Course, 40, 10 p.

Nabelek, P.I., Whittington, A.G., and Sirbescu, M.C. (2010) The role of H_2O in rapid emplacement and crystallization of granite pegmatites: resolving the paradox of large crystals in highly undercooled melts. Contributions to Mineralogy and Petrology, 160, 313–325.

696 Newton, R.C., and Manning, C.E. (2006) Solubilities of corundum, wollastonite and
697 quartz in H_2O–NaCl solutions at 800. Geochimica et Cosmochimica Acta, 70,
698 5571–5582.
699 Rockhold, J.R., Nabelek, P.I., and Glascock, M.D. (1987) Origin of rhythmic layering in
700 the Calamity Peak satellite pluton of the Harney Peak Granite, South Dakota.
701 Geochimica et Cosomochimica Acta., 136, 310–330.
702 Sirbescu, M.C., and Nabelek, P.I. (2003a) Crustal melts below 400 ºC. Geology, 31, 685–
703 688.
704 Sirbescu, M.C., and Nabelek, P.I. (2003b) Crystallization conditions and evolution of
705 magmatic fluids in the Harney Peak Granite and associated pegmatites, Black
706 Hills, South Dakota—Evidence from fluid inclusions. Geochimica et
707 Cosmochimica Acta, 67, 2443–2465.
708 Sirbescu, M.C., Hartwick, E.E., and Student, J.J. (2008) Rapid crystallization of the
709 Animikie Red Ace Pegmatite, Florence county, northeastern Wisconsin:
710 inclusions microthermometry and conductive-cooling modeling. Contributions to
711 Mineralogy and Petrology, 156, 289–305.
712 Smith, T.E., Huang, C.H., Walawender, M.J., Cheung, P., and Wheeler, C. (1983) The
713 gabbroic rocks of the Peninsular Ranges batholith, southern California: cumulate
714 rocks associated with calc-alkalic basalts and andesites. Journal of Volcanology
715 and Geothermal Research, 18, 249–278.
716 Stern, L.A., Brown, G.E., Bird, D.K., Jahns, R.H., Foord, E.F., Shigley, J.E., and
717 Spaulding, L.B. (1986) Mineralogy and geochemical evolution of the Little Three

718 pegmatite-aplite layered intrusion, Ramona, California. American Mineralogist,
719 71, 406–427.
720 Symons, D.T.A., Walawender, M.J., Smith, T.E., Molnar, S.E., Harris, M.J., and
721 Blackburn, W.H. (2003) Paleomagnetism and geobarometry of the La Posta
722 pluton, California. Geological Society of America: Special Paper, 374, 135–155.
723 Symons, D.T.A., Smith, T.E., Kawasaki, K., and Walawender, M.J. (2009)
724 Paleomagnetism of the mid-Cretaceous gem-bearing pegmatite dikes of San
725 Diego County, California, USA. Canadian Journal of Earth Sciences, 46, 675–
726 687.
727 Taylor, B.E., Foord, E.E., Friedrichsen, H. (1979) Stable isotopes and fluid inclusion
728 studies of GEM-bearing granitic pegmatite-aplite dikes, San Diego Co.,
729 California. Contributions to Mineralogy and Petrology, 68, 187–205.
730 Thomas, R., and Davidson P. (2012) Water in granite and pegmatite-forming melts. Ore
731 Geology Reviews, 46, 32–46.
732 Veksler, I.V., and Thomas, R. (2002) An experimental study of B-, P- and F-rich
733 synthetic granite pegmatite at 0.1 and 0.2 GPa. Contributions to Mineralogy and
734 Petrology, 143, 673–683.
735 Walawender, M.J., and Smith, T.E. (1980) Geochemical and petrologic evolution of the
736 basic plutons of the Peninsular Ranges Batholith, southern California. The Journal
737 of Geology, 88, 233–242.
738 Webber, K.L., Simmons, W.B., Falster, A.U., and Foord, E.E. (1999) Cooling rates and
739 crystallization dynamics of shallow lever pegmatite-aplite dikes, San Diego
740 County, California. American Mineralogist, 84, 708–717.

741 Webber, K.L., Falster, A.U., Simmons, W., and Foord, E.E. (1997) The role of diffusion-
742 controlled oscillatory nucleation in the formation of line rock in pegmatite-aplite
743 dikes. Journal of Petrology**,** 38, 1777–1791.

744 Wetmore, P.H., Schmidt, K.L., Paterson, S.R., and Herzig, C. (2002) Tectonic
745 implications for the along-strike variation of the Peninsular Ranges batholith,
746 southern and Baja California. Geology, 30, 247–250.
747 Whittington, A.G., Bouhifd, M.A., and Richet, P. (2009) The viscosity of hydrous
748 $NaAlSi_3O_8$ and granitic melts: Configurational entropy models. American
749 Mineralogist, 94, 1–16.
750 Williams, A.E., and Taylor, M.C. (1996) Mass spectrometric identification of boric acid
751 in fluid inclusions in pegmatite minerals. Geochimica et Cosmochimica Acta, 60,
752 3435–3443.
753 Wohlers, A., Manning, C.E., and Thompson, A.B. (2011) Experimental investigation of
754 the solubility of albite and jadeite in H_2O, with paragonite+quartz at 500 and
755 600°C, and 1–2.25 GPa. Geochimica et Cosmochimica Acta, 75, 2924–2939.
756 Xu, H., Heaney, P.J., and Navrotsky, A. (2001) Thermal expansion and structural
757 transformations of stuffed derivatives of quartz along the $LiAlSiO_4$–SiO_2 join: a
758 variable-temperature powder synchrotron XRD study. Physics and Chemistry of
759 Minerals, 28, 302–312.
760
761
762
763

764 **Figure Captions**

765 **Figure 1.** Sketch of San Diego County, California (after Fisher 2002). The larger squares
766 represent sample districts, labeled Jacumba (La Posta pegmatite) and Mesa Grande
767 (Himalaya pegmatite). The other major districts described by Fisher (2002) are also
768 shown with smaller squares and numbered as follows: Vista–Moosa Canyon (1), Rincon
769 (2), Aguanga Mountain (3), Chihuahua Valley (4), Ramona (5), Banner (6), and Pala (7).
770

771 **Figure 2.** CL images (scale bar represents 1 mm) of various common minerals in
772 pegmatites: (a) red muscovite/lepidolite, (b) alteration of quartz adjacent to fractures
773 (blue); pink is lepidolite, note that this image has a particularly high exposure (5
774 seconds), which causes the fractures to appear white due to over-exposure; (c) microcline
775 alteration (brown), (d) lepidolite (pink) within and around tourmaline.
776

777 **Figure 3.** Examples of fluid inclusions microphotographs of (a) primary inclusions and
778 (b) secondary inclusions from the Himalaya and La Posta pegmatites.
779

780 **Figure 4.** (a) Plot of measured homogenization temperature (T_h) of fluid inclusions (to
781 liquid) versus measured eutectic melting temperature (T_e) for primary and secondary
782 inclusions in the Himalaya pegmatite core zone. (b) Plot of measured homogenization
783 temperature of fluid inclusions (to liquid) versus measured eutectic melting temperature
784 for primary and secondary inclusions in the core and intermediate zone of the La Posta
785 pegmatite.
786

Figure 5. LA-ICP-MS data showing relative atomic proportions of Li–Na–B and Ca–Na–B in primary and secondary fluid inclusions in the Himalaya (a and b) and La Posta (c and d) pegmatites.

Figure 6. Plot of average F^-/Cl^- versus SO_4^{2-}/Cl^- ratios in fluid inclusions in single leachates in the Himalaya and La Posta pegmatites.

Figure 7. Calculated plots showing stability fields of some key minerals that occur in walls and insides of pockets in (a) $\log(a_{Na+}/a_{H+})$-temperature and (b) $\log(a_{K+}/a_{H+})$-temperature diagrams, calculated for 200 MPa. Gray arrows show inferred change in conditions during transition from magmatic to hydrothermal stages of crystallization.

Figure 1

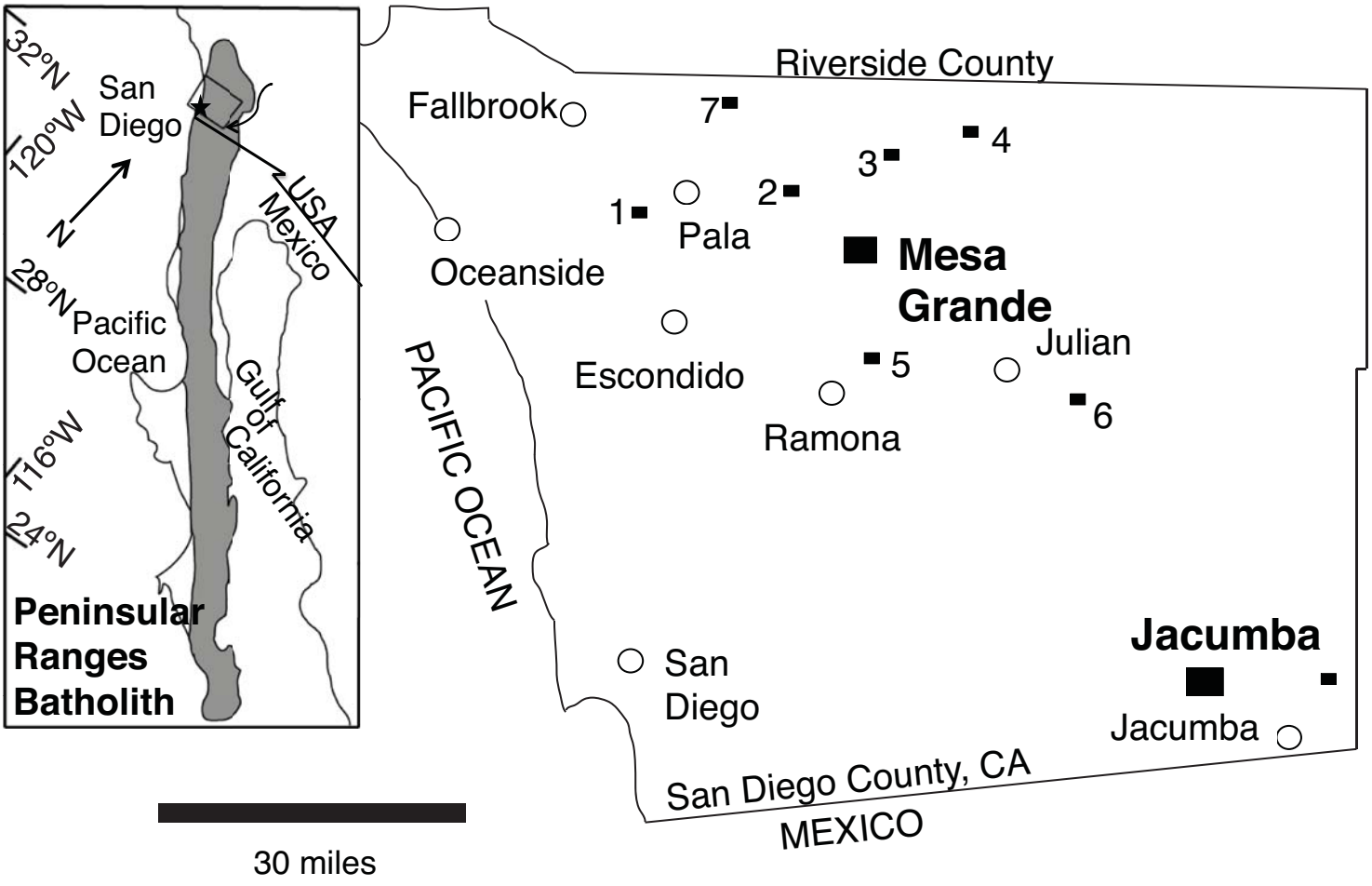
32°N
120°W
San Diego
N
USA
Mexico
28°N
Pacific Ocean
Gulf of California
116°W
24°N
Peninsular Ranges Batholith
Riverside County
Fallbrook
7
4
3
2
1
Pala
Mesa Grande
Oceanside
Julian
Escondido
5
6
Ramona
PACIFIC OCEAN
Jacumba
San Diego
Jacumba
San Diego County, CA
MEXICO
30 miles

Figure 2

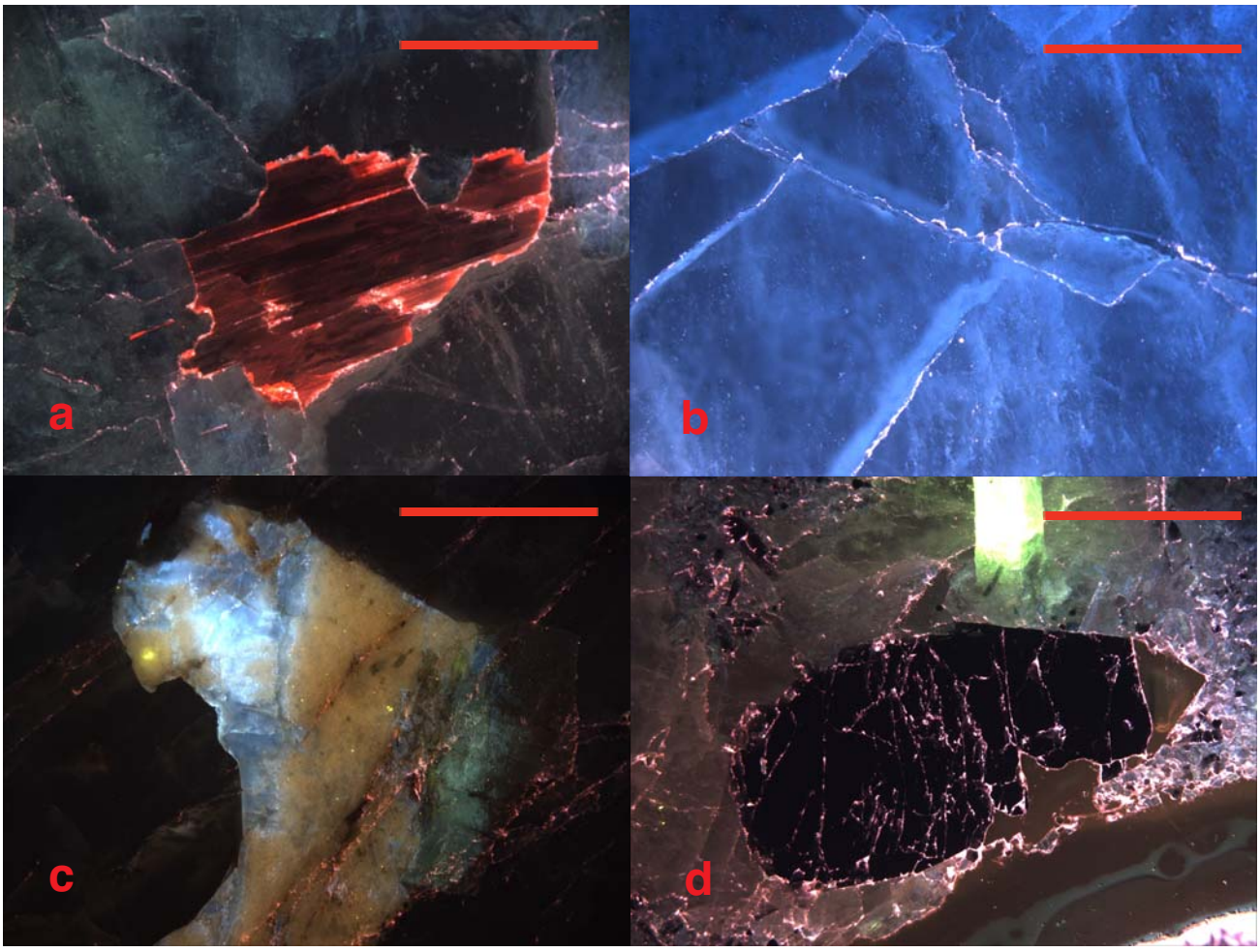

Figure 3

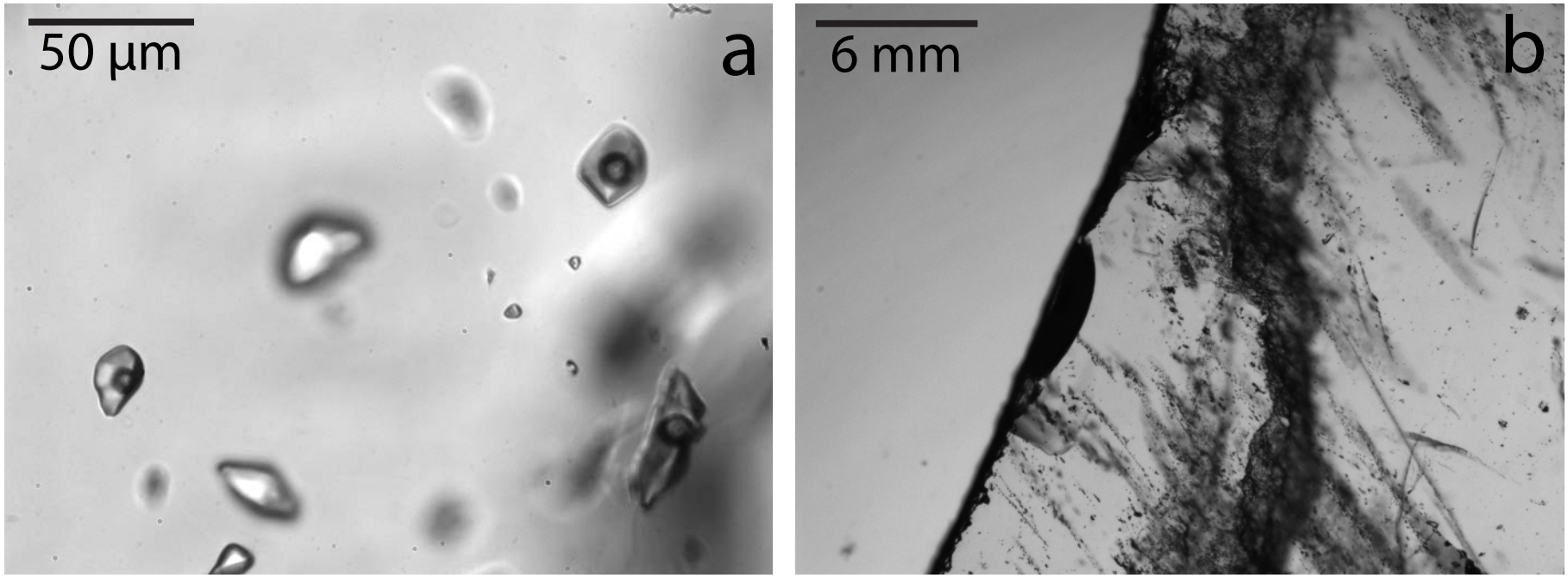

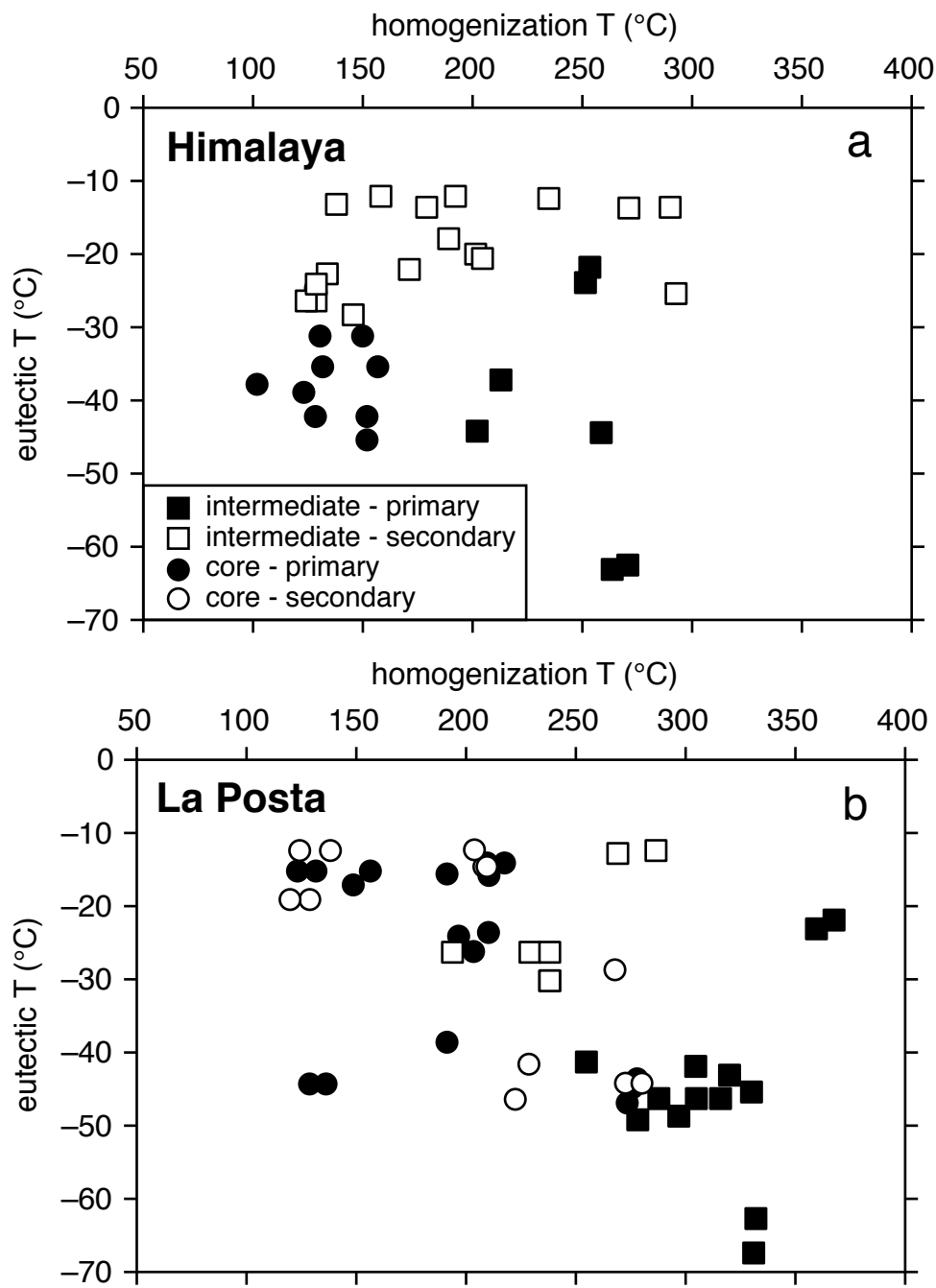
homogenization T (°C)
50
100
150
200
250
300
350
400
0
−10
−20
−30
−40
−50
−60
−70
eutectic T (°C)
Himalaya
a
intermediate - primary
intermediate - secondary
core - primary
core - secondary
homogenization T (°C)
50
100
150
200
250
300
350
400
0
−10
−20
−30
−40
−50
−60
−70
eutectic T (°C)
La Posta
b

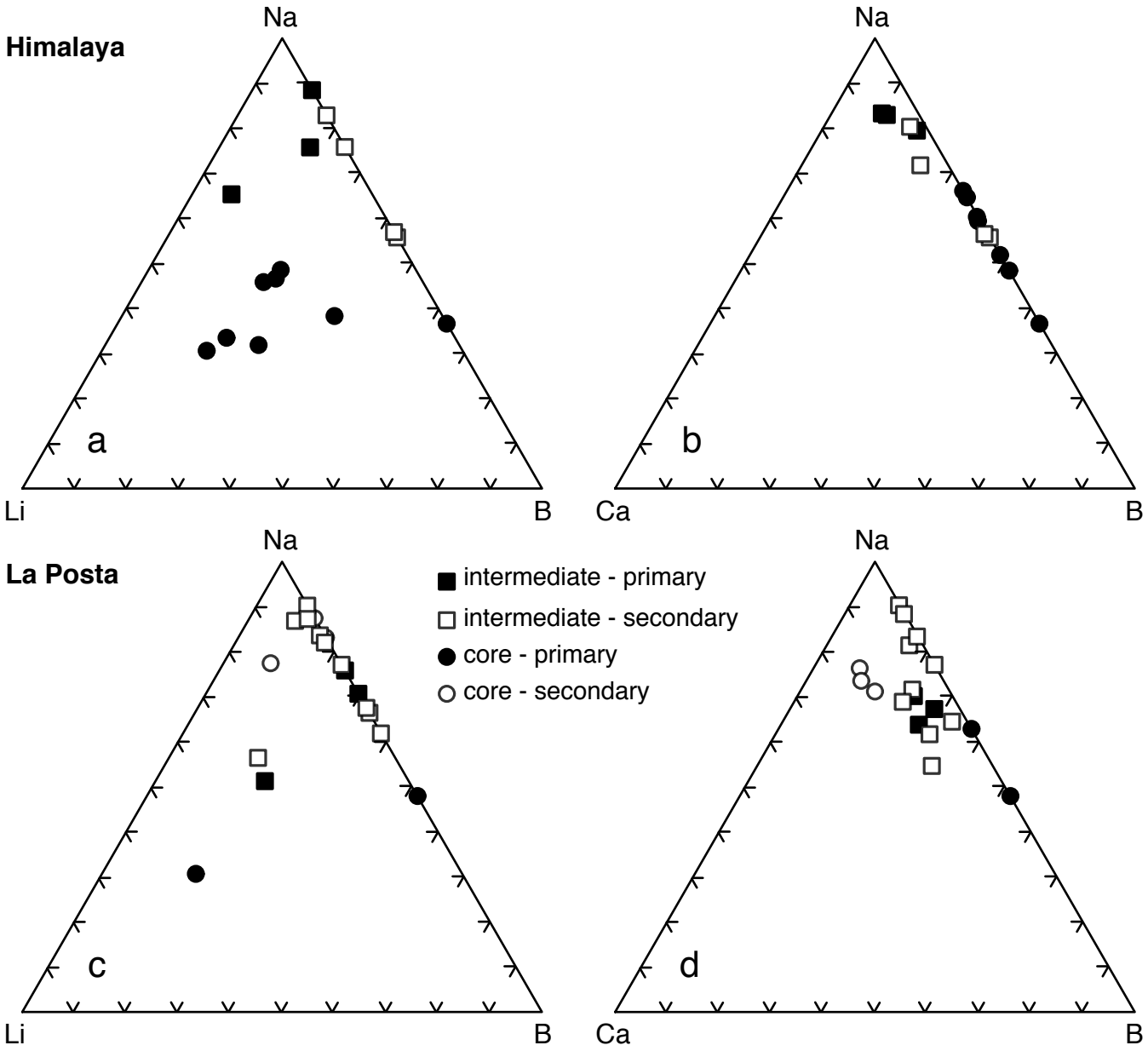
Himalaya
Na
Li
B
a
Na
Ca
B
b
La Posta
Na
Li
B
c
Na
Ca
B
d
intermediate - primary
intermediate - secondary
core - primary
core - secondary

Figure 5

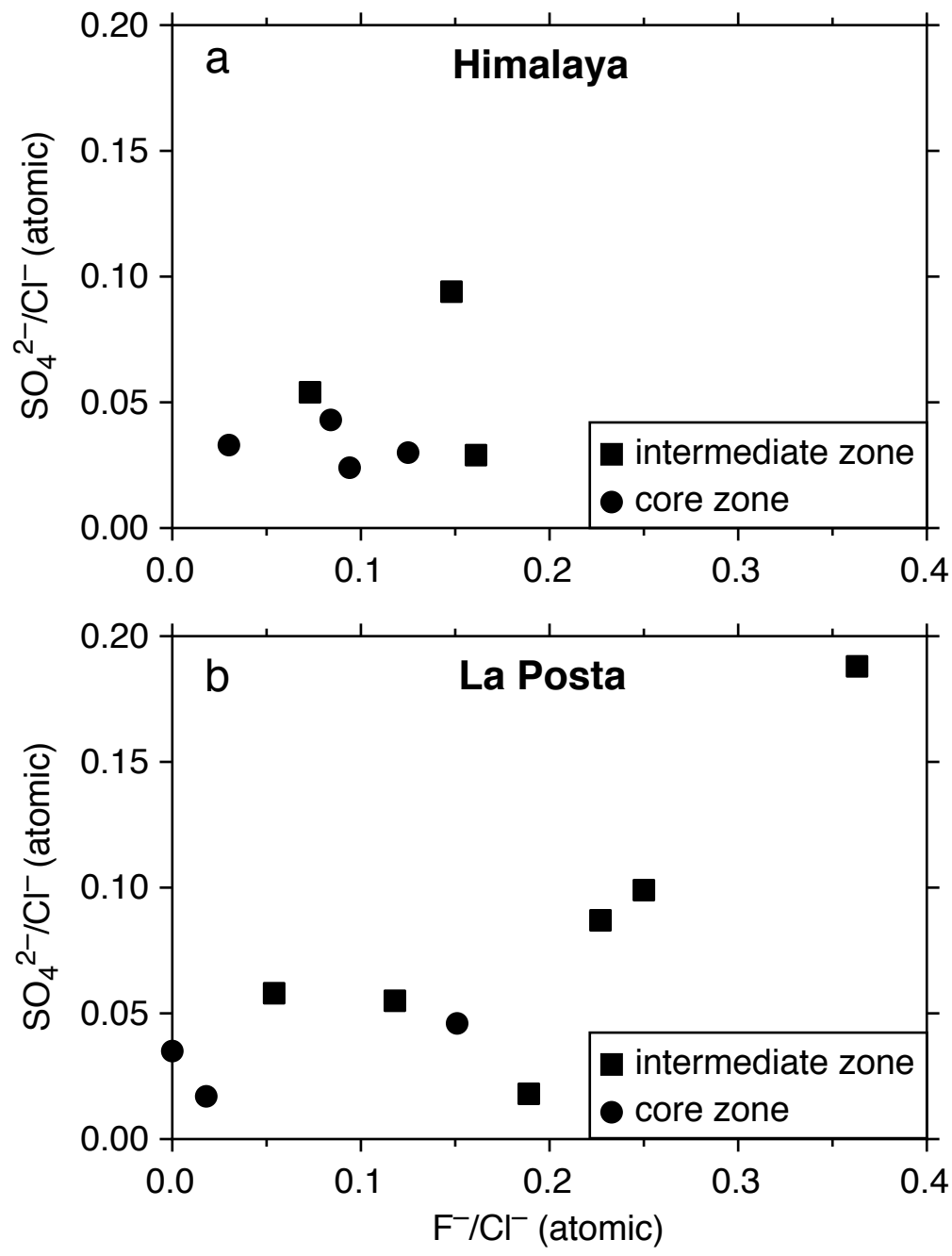
a
Himalaya
SO_4^{2-}/Cl^- (atomic)
0.20
0.15
0.10
0.05
0.00
0.0
0.1
0.2
0.3
0.4
intermediate zone
core zone
b
La Posta
SO_4^{2-}/Cl^- (atomic)
F^-/Cl^- (atomic)
intermediate zone
core zone

Figure 7

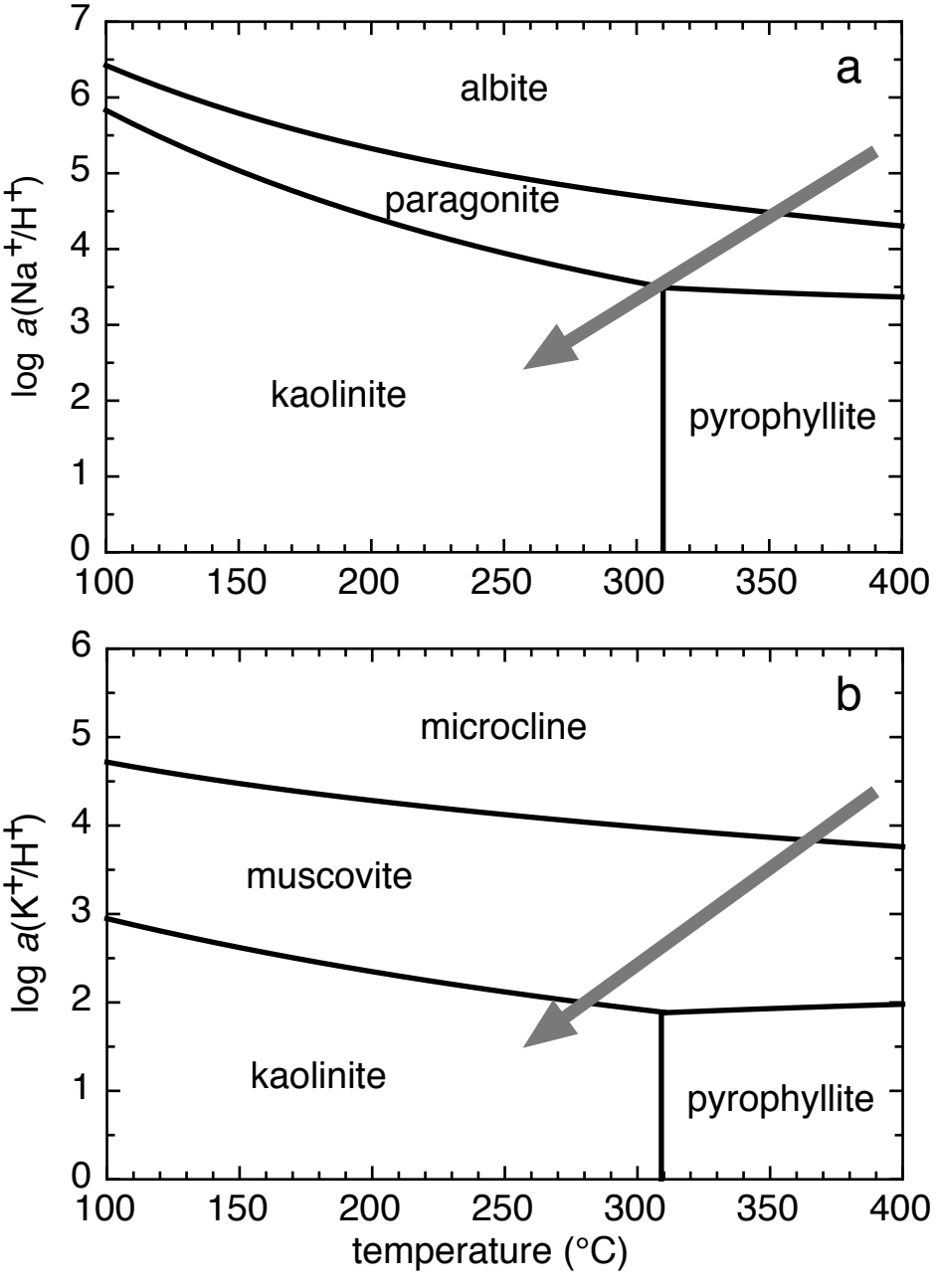
a
albite
paragonite
kaolinite
pyrophyllite
log a(Na+/H+)
b
microcline
muscovite
kaolinite
pyrophyllite
log a(K+/H+)
temperature (°C)